AGU PUBLICATIONS

Geophysical Research Letters

RESEARCH LETTER
10.1002/2014GL059589

Key Points:
- Interannual upwelling variability is studied from modeled vertical velocity
- Nearshore (<50 km) and offshore (50–200 km) upwelling variability are out of phase
- Cross-shelf upwelling structure is coupled to large-scale climate variability

Correspondence to:
M. G. Jacox,
mjacox@ucsc.edu

Citation:
Jacox, M. G., A. M. Moore, C. A. Edwards, and J. Fiechter (2014), Spatially resolved upwelling in the California Current System and its connections to climate variability, *Geophys. Res. Lett.*, *41*, doi:10.1002/2014GL059589.

Received 12 FEB 2014
Accepted 15 APR 2014
Accepted article online 22 APR 2014

Spatially resolved upwelling in the California Current System and its connections to climate variability

M. G. Jacox[1], A. M. Moore[1], C. A. Edwards[1], and J. Fiechter[1]

[1]Department of Ocean Sciences, University of California, Santa Cruz, California, USA

Abstract A historical analysis of California Current System (CCS) circulation, performed using the Regional Ocean Modeling System with four-dimensional variational data assimilation, was used to study upwelling variability during the 1988–2010 period. We examined upwelling directly from the vertical velocity field, which elucidates important temporal and spatial variability not captured by traditional coastal upwelling indices. Through much of the CCS, upwelling within 50 km of the coast has increased, as reported elsewhere. However, from 50 to 200 km offshore, upwelling trends are negative and interannual variability is 180° out of phase with the nearshore signal. This cross-shore pattern shows up as the primary mode of variability in central and northern CCS vertical velocity anomalies, accounting for ~40% of the total variance. Corresponding time series of the dominant modes in the central and northern CCS are strongly correlated with large-scale climate indices, suggesting that climate fluctuations may alternately favor different biological communities.

1. Introduction

Upwelling off the West Coast of North America supports rich and diverse biological communities of considerable ecological and socioeconomic importance in the California Current System (CCS). As such, much effort has been expended in understanding the drivers of upwelling variability and trends, and in predicting the evolution of the CCS in a changing climate. *Bakun* [1990] hypothesized an increase in upwelling favorable winds under atmospheric warming scenarios due to intensification of the land-sea pressure gradient, a hypothesis supported by observational studies covering recent decades [*García-Reyes and Largier*, 2010; *Seo et al.*, 2012]. At the same time, a deepening and strengthening of the seasonal thermocline [*Palacios et al.*, 2004; *Di Lorenzo et al.*, 2005] reduces the efficacy of upwelling for bringing deep nutrients to the ocean's sunlit surface layer. Trends in stratification and equatorward winds are therefore expected to have opposing impacts on the biological response, and it is unclear which effect is dominant on long time scales [*Di Lorenzo et al.*, 2005; *Auad et al.*, 2006].

Several basin-scale climate indices have been linked to important shifts in CCS biology: El Niño–Southern Oscillation (ENSO) [*Bograd and Lynn*, 2001], the Pacific Decadal Oscillation (PDO) [*Chavez et al.*, 2003], and the North Pacific Gyre Oscillation (NPGO) [*Di Lorenzo et al.*, 2008]. Recently, dominant climate modes have been linked more specifically to interannual variability in upwelling intensity. For example, *Macías et al.* [2012] found that upwelling intensity correlates with ENSO and the PDO through much of the CCS, and with the NPGO in the central CCS. *Chenillat et al.* [2012] reported further that the timing of seasonal upwelling onset in the central CCS is modulated by fluctuations in the NPGO. In both studies, due to the absence of in situ vertical velocity time series, upwelling intensity was approximated by pressure-based wind estimates. In this paper, we examine upwelling using a data-assimilative model to estimate the ocean circulation in the CCS over the past 30 years. A key result is that temporal variability in upwelling is associated with coherent cross-shore structure that is not captured by traditional upwelling proxies.

2. Numerical Model

The circulation analyses were computed using the Regional Ocean Modeling System four-dimensional variational (ROMS 4D-Var) data assimilation system [*Moore et al.*, 2011a, 2011b] in the dual formulation. The present study was configured with 42 vertical levels, 0.1° horizontal resolution, and 8 day assimilation cycles. *Moore et al.* [2013] provide a complete description of the configuration of the system, which uses available observations to correct surface forcing, initial conditions, and boundary conditions. The model

©2014. American Geophysical Union. All Rights Reserved.

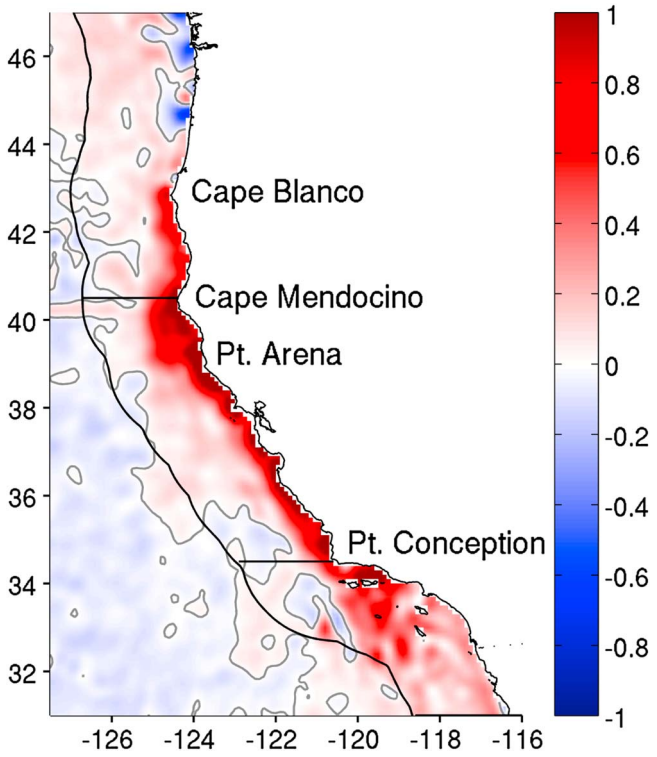

Figure 1. Mean model vertical velocity ($\overline{w}$, m/d). The grey contour indicates $\overline{w} = 0$. The domain is divided into northern, central, and southern regions, with divisions at Cape Mendocino and Point Conception. Mean upwelling conditions ($\overline{w} > 0$) extend ~200 km from shore (black contour).

domain extends from northern Washington State in the north to midway down the Baja Peninsula in the south. In a very similar model configuration without assimilation, *Veneziani et al.* [2009] found accurate representation of the mean and seasonal cycle of circulation features off the California coast, and *Broquet et al.* [2009] showed that 4D-Var further improves the circulation characteristics in our domain. Figure 1 shows the coastal band of interest to this study. We divide the model domain into northern, central, and southern regions with divisions at Cape Mendocino and Point Conception, which mark significant transitions in both the coastline orientation and the nature of the wind forcing [*Dorman and Winant*, 1995].

In order to compute the best circulation estimates, the model assimilates satellite data (Advanced Very High Resolution Radiometer (AVHRR) Pathfinder, Advanced Microwave Scanning Radiometer-EOS (AMSR-E) and Moderate Resolution Imaging Spectroradiometer (MODIS) Terra for sea surface temperature (SST), Archiving, Validation, and Interpretation of Satellite Oceanographic data (AVISO) for sea surface height (SSH)), and in situ measurements of temperature and salinity (expendable bathythermographs, mechanical bathythermographs, conductivity-temperature-depth sensors, and Argo profiling floats from version 2a of the quality-controlled ENSEMBLES (EN3) data set [*Ingleby and Huddleston*, 2007]).

Surface forcing is from the European Centre for Medium-Range Weather Forecasting 40 year reanalysis (ERA 40) for 1980–2001, ERA Interim for 2002–2010, and the cross-calibrated multiplatform (CCMP) wind product of *Atlas et al.* [2011] for 1988–2010. ERA 40 was used during the initial 22 years in place of the higher-resolution ERA Interim product in order to maintain consistency between the surface heat and freshwater fluxes and the CCMP wind product, which used ERA 40 as the prior. While the model integration spans 1980–2010, we focus our analysis on the 1988–2010 period in which the cross-shore profile of surface winds is resolved by relatively high resolution (0.25°) CCMP winds.

3. Upwelling Estimation

Upwelling intensity is typically estimated by the coastal upwelling index (CUI) [*Bakun*, 1973], calculated from atmospheric sea level pressure fields. A full description of the CUI methodology and important caveats is presented by *Schwing et al.* [1996]. As a readily available product, the CUI is an invaluable resource that has been used in studies on topics ranging from the dynamics of the CCS to upwelling impacts on biology at all trophic levels from phytoplankton to whales. In the present study, however, we diagnose upwelling directly from the three-dimensional model velocity field. This approach has several distinct advantages of particular relevance here: (i) Spatial patterns can be better resolved, including important variability along shore (e.g., upwelling intensification downstream of capes) and cross shore (e.g., nearshore coastal divergence versus offshore wind stress curl-driven upwelling), (ii) uncertainties associated with estimating the alongshore wind from atmospheric pressure fields are eliminated, and (iii) the model dynamics implicitly account for

©2014. American Geophysical Union. All Rights Reserved.

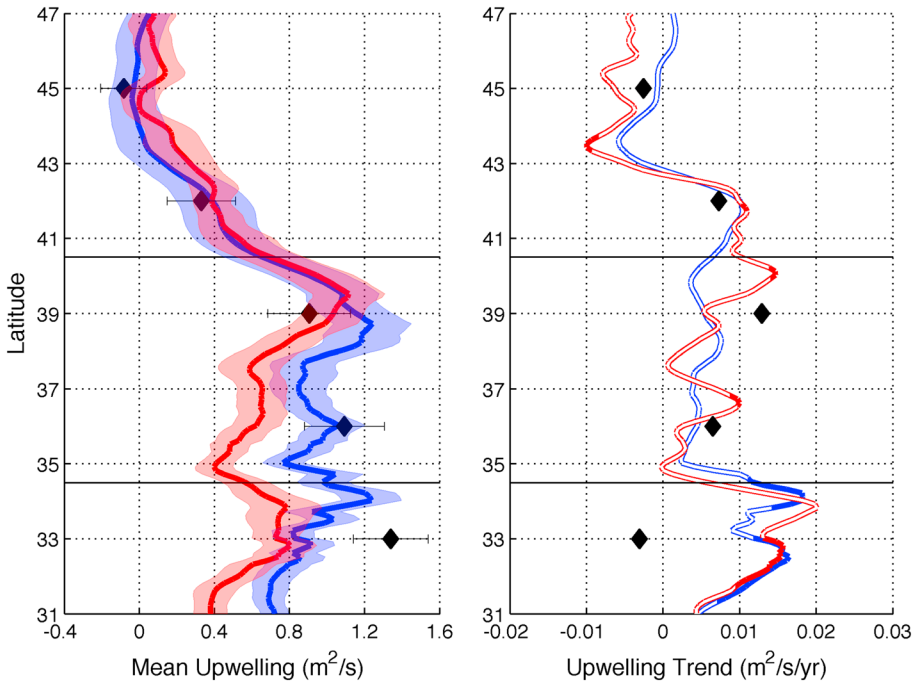

Figure 2. (left) Mean and (right) trend of upwelling transport estimated from CCMP winds (blue), ROMS vertical velocities (red), and CUI (black diamonds). ROMS transports are calculated for a 200 km wide coastal band, and a 1° latitudinal smoothing is applied. Shaded regions (for ROMS) and error bars (for CUI) indicate the standard deviation of annual means. Open lines indicate trends with $p > 0.05$. Horizontal lines mark regional divisions at Cape Mendocino (40.5°N) and Point Conception (34.5°N).

significant discrepancies between Ekman transport and upwelling transport due to net onshore geostrophic flow [*Marchesiello and Estrade*, 2010].

We calculate upwelling transport by spatially integrating the vertical velocity at 40 m depth, which is the space-time mean mixed layer depth (MLD) in our domain. The choice of a fixed depth allows for unambiguous calculation of transport budgets like those in Figure 3. While the actual MLD varies substantially, vertical transport though 40 m is highly correlated with transport through the MLD in our study area ($r = 0.95$), and both capture the same long-term trends. Model transports reported in this paper were recorded every 6 h, monthly averaged, and spatially smoothed with three iterations of a 1-2-1 filter. Finally, as the present study is concerned with variability on interannual-to-decadal scales, a 12 month running mean was applied to filter out the seasonal cycle in ROMS output as well as climate indices. The running mean produces time series that are qualitatively similar to alternatives such as removing a mean seasonal cycle or the first two harmonics but are less sensitive to changes in seasonal timing. For significance calculations, autocorrelation in the smoothed monthly data was accounted for in the effective degrees of freedom $N_e = N\Delta t/\tau$, where N is the number of data points regularly spaced in time at interval Δt and τ is the time lag at which autocorrelation crosses zero. Unless indicated otherwise, reported correlations and trends are significant at the 95% level or higher.

4. Meridional Trends and Variability

Figure 2 shows the 1988–2010 mean and linear trend of model vertical transport integrated over a 200 km wide coastal band in which long-term mean vertical velocities are positive (net upwelling) for much of the CCS (Figure 1). Mean upwelling transport is weakest in the northern CCS, where downwelling conditions prevail over much of the year. The greatest total upwelling is observed in the lee of major coastal promontories (Cape Mendocino, Point Arena, Point Conception). A positive upwelling trend in the Southern California Bight (SC Bight) is equal to 2–4% of the 1988–2010 mean per year. Thus, the local change in upwelling intensity from 1988 to 2010 is comparable to the mean value for the period. In the north of the domain, the standard deviation of annual mean vertical transport crosses zero, indicating that some years are

©2014. American Geophysical Union. All Rights Reserved.

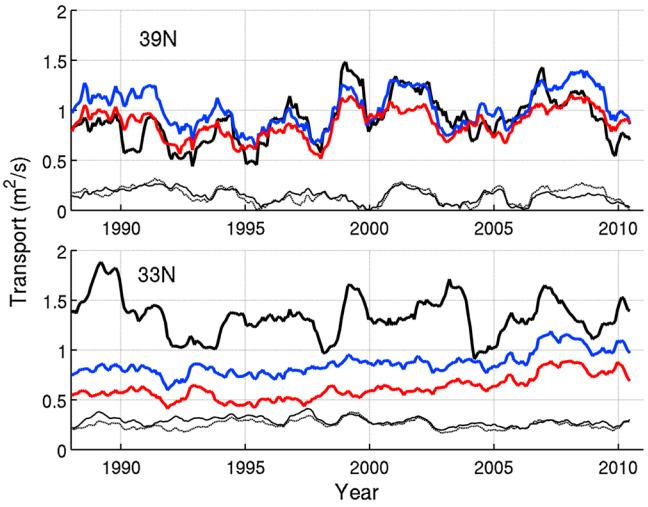

Figure 3. Time series of upwelling estimates from the CUI (black), CCMP winds (blue), and ROMS vertical velocities (red) at (top) 39°N and (bottom) 33°N. The dashed line is the difference between Ekman transport (blue) and vertical transport (red), which is accounted for by onshore geostrophic flow (thin black line). Quantities are calculated as in Figure 2, and ROMS values are averaged over 3° of latitude for consistency with the CUI.

predominantly upwelling while others favor downwelling. A negative trend north of Cape Blanco (~43°N) indicates an increasing prevalence of net downwelling years in the latter part of our study period. A positive upwelling trend is visible throughout much of the central CCS, though statistically significant trends emerge in only a few small areas.

Model upwelling and wind-derived estimates agree well in the northern region but diverge south of 39°N (Figure 2). Differences between the CUI (black) and upwelling transport (red) have two sources: (i) net onshore geostrophic flow that suppresses upwelling [*Marchesiello and Estrade*, 2010] and (ii) differences between observation-based estimates of the wind (CCMP) and pressure-based estimates. The first of these two sources is dominant off the central California coast, where both the CUI and Ekman transport overestimate upwelling by as much as 100%. In contrast, at 33°N Ekman transport is much less than the CUI, indicating the significance of source (ii) in the SC Bight. *Bakun* [1973] anticipated this issue due to the effect of the coastal mountain range in Southern California.

Trends in all three upwelling metrics (CUI, Ekman transport, and vertical transport) are largely consistent north of the SC Bight (Figure 2). Figure 3 shows time series of each metric at two latitudes where the CUI is available. At 39°N, the CUI is a good indicator of mean upwelling transport and also captures interannual variability; vertical transport and the CUI are significantly correlated at $r = 0.69$. Discrepancies between Ekman transport and upwelling transport are consistent with calculated onshore geostrophic flow, which is variable in time but less than 20% of the upwelling magnitude. At locations where the long-term mean CUI and model upwelling diverge (33 and 36°N), we also find that they are not significantly correlated ($r < 0.3$). However, Ekman transport is strongly correlated with upwelling transport at all five locations ($r = 0.84$–0.95), so interannual changes in the CUI-upwelling discrepancy are driven more by wind estimates than by the geostrophic flow. Though onshore geostrophic flow is relatively strong off central and southern California, it has little interannual variability. Ekman transport therefore tracks upwelling transport, but on average is biased high by 41% at 33°N and 60% at 36°N.

The lack of a significant upwelling trend in the central CCS (Figure 2) is in contrast with prior analyses of upwelling favorable winds and sea surface temperature that suggest increased upwelling in the region [*Schwing and Mendelssohn*, 1997; *García-Reyes and Largier*, 2010; *Seo et al.*, 2012]. However, trends in model upwelling shown in Figure 2 are indicative of changes across the entire width of the coastal upwelling band and do not distinguish intense nearshore upwelling from weaker upwelling farther offshore. We therefore expand our analysis using empirical orthogonal functions (EOFs) of vertical velocity anomaly w' to examine 2-D patterns in upwelling variability and their evolution in time.

5. Dominant Upwelling Modes

In both the northern and central CCS, the primary mode of variability accounts for ~40% of the variance and captures a distinct cross-shore gradient with a sign change approximately 50 km from shore (Figure 4). Since low-pass filtering of velocities was performed prior to calculating EOFs, this pattern is representative of interannual variability, not the seasonal cycle in coastal upwelling. In the northern region, EOF2 accounts for 11% of the variance and captures an alongshore dipole pattern in the upwelling variability nearshore, with a

©2014. American Geophysical Union. All Rights Reserved.

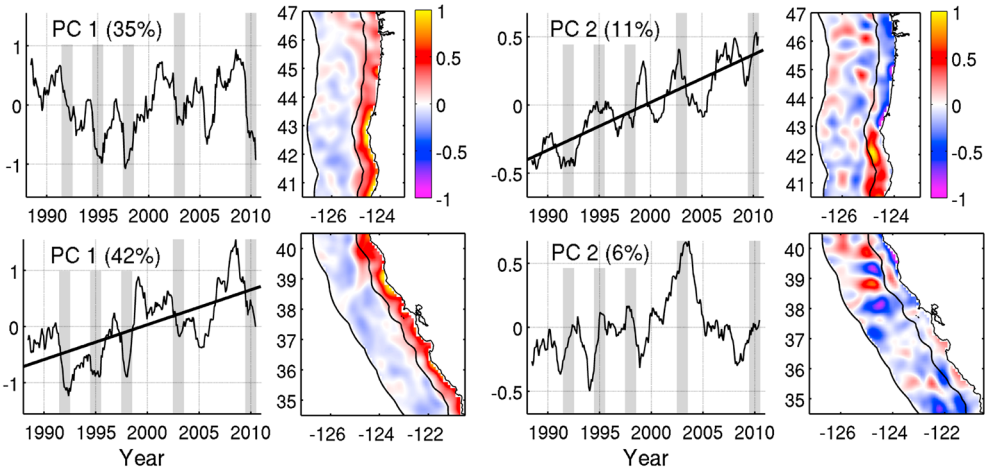

Figure 4. (first and third columns) First and second principal components (PCs) and (second and fourth columns) EOFs of vertical velocity anomaly (m/d) for the (top) northern and (bottom) central CCS regions. Thick black lines indicate trends significant at the 95% level or higher. Contours 50 and 200 km from shore mark the approximate location of the EOF sign change and the offshore extent of mean upwelling, respectively. The explained variance for each mode is given in parentheses, and grey bars mark El Niño years.

sign change at 43°N. EOF2 for the central CCS accounts for just 6% of the variance and does not exhibit any clear spatial coherence.

Principal component (PC) time series show strong temporal variability in EOF1 throughout the central and northern CCS, including clear reductions in nearshore upwelling during strong El Niño years (discussed further in section 6). The significant positive trend in central CCS PC1 captures a pattern that is also present in the full upwelling signal: increased upwelling transport nearshore (consistent with prior analyses) and decreased upwelling in a broader region from 50 to 200 km offshore. The net effect is a small positive upwelling trend from Point Conception to Cape Blanco (Figure 2), indicating dominance of the nearshore (<50 km) signal in determining overall upwelling transport. In the northern CCS, no significant trend emerges in PC1; however, there is a significant positive trend in PC2, which indicates increased nearshore upwelling south of Cape Blanco and decreased upwelling to the north.

In the southern region (not shown), the leading mode of variability accounts for 24% of the variance and captures significantly increased upwelling throughout much of the SC Bight, consistent with Figure 2. The increase is especially pronounced immediately south of Point Conception. As in the central and northern regions, the nearshore increase is accompanied by a decrease farther offshore, though the nearshore/offshore division in the south is not as clear-cut as it is elsewhere.

6. Climate Variability

Three basin-scale climate modes, the PDO, the NPGO, and ENSO, have been implicated as important controls on CCS upwelling. ENSO variability is described here by the multivariate ENSO index (MEI), the first principal component of six combined atmospheric and oceanic variables in the tropical Pacific [*Wolter and Timlin*, 1993]. The PDO emerges as the dominant mode of variability in North Pacific SST [*Mantua et al.*, 1997], while the NPGO is the second leading mode of SSH variability in the northeast Pacific [*Di Lorenzo et al.*, 2008]. We examine here their relationships with key modes of upwelling variability described in section 5.

Strong ENSO events impact the biochemical response to upwelling in the central CCS through modulation of both the seasonal thermocline depth [*Chavez et al.*, 2002] and the strength of nearshore upwelling-favorable winds [*Schwing et al.*, 2002]. During El Niño conditions, a deep thermocline and anomalously weak equatorward winds reduce the efficacy of upwelling for delivering nutrients to the euphotic zone. In our model results, the signature of El Niño events is clearly visible in the primary mode of upwelling variability (Figure 4). The MEI is strongly correlated with PC1 in the central CCS ($r = -0.69$), and less so in the northern region ($r = -0.42$, $p = 0.06$), while correlations in the south are weaker and not statistically significant. Negative correlations in the northern and central regions imply reduced upwelling during El Niño in a

©2014. American Geophysical Union. All Rights Reserved.

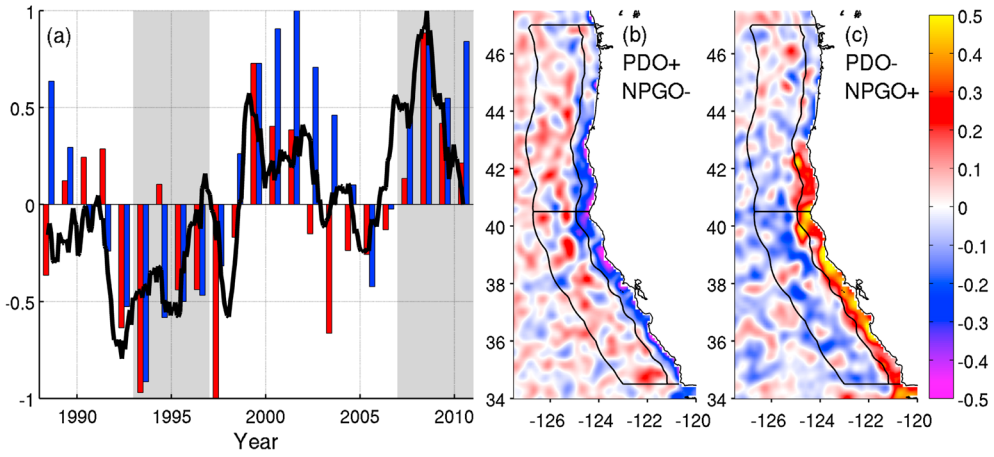

Figure 5. (a) PC1 of vertical velocity anomaly in the central CCS (black line) with annual means of the NPGO (red) and the PDO (sign reversed, blue), each normalized to a maximum magnitude of one. Grey bars mark 1993–1996 and 2007–2010, positive (negative) and negative (positive) phases of the PDO (NPGO), respectively. (b and c) Corresponding mean vertical velocity anomalies for each of the two periods. Contours are as in Figure 4.

~50 km wide coastal band north of Point Conception, consistent with buoy observations [*García-Reyes and Largier*, 2012]. However, our results also indicate increased upwelling transport farther offshore (50–200 km) when El Niño conditions prevail, a result that to our knowledge has not been previously reported. When integrating transport over the full width of the upwelling band, we find that the nearshore signal is dominant and positive MEI periods are generally accompanied by relatively weak upwelling (Figure 3, top). Any offshore upwelling increase is therefore obscured, consistent with a negative correlation between the CUI and MEI [*Macías et al.*, 2012].

In addition to an association with ENSO, we find upwelling variability to be tightly coupled to decadal-scale climate indices. PC1 correlates significantly with the PDO in the northern CCS ($r = -0.55$), and with both the PDO ($r = -0.71$) and NPGO ($r = 0.60$) in the central CCS. Again, no significant correlations were found in the southern CCS. The correlation of PC1 with decadal-scale climate indices, and the nearshore/offshore gradient captured by EOF1, manifest in the vertical velocity field as shown in Figure 5. Upwelling transport from 50 to 200 km offshore is reduced during periods of increased nearshore (<50 km) upwelling intensity, and vice versa. In our study period, the PDO and NPGO are negatively correlated with each other, so Figure 5 highlights periods of sustained positive/negative PDO, which overlap negative/positive NPGO phases. Mean nearshore vertical transport during the PDO+/NPGO− phase is 71% (24%) less than the 1988–2010 mean in the northern (central) region, while offshore vertical transport is 36% (23%) greater. In the PDO−/NPGO+ phase, nearshore transport is 25% (34%) greater than the long-term mean while offshore transport is 17% (45%) less.

7. Discussion

We analyzed upwelling along the US West Coast from vertical velocities in a data-assimilative ocean model that represents our best estimate of the ocean state over the past quarter century. Though mean upwelling conditions ($\overline{w} > 0$) extend approximately 200 km from shore, upwelling variability is not coherent across the 200 km band. Significantly, increased upwelling transport within 50 km of the coast is consistent with a recent cooling trend in buoy SST measurements [*García-Reyes and Largier*, 2010; *Seo et al.*, 2012] and is captured by the first mode of variability in vertical velocity anomalies. However, when integrating vertical velocities over the full width of the upwelling band, variability in the nearshore signal is partially compensated by changes of opposite sign farther offshore (50–200 km). This cross-shore structure of upwelling variability is an important and previously unreported result, suggesting that caution be exercised when evaluating upwelling from point measurements (e.g., buoys) or integrated measures (e.g., the CUI) that are not representative of the entire upwelling band.

Note that the nearshore/offshore bands described here are not intended to be coincident with distinct upwelling mechanisms. The offshore extent of upwelling due to divergence at the coastal boundary is often

©2014. American Geophysical Union. All Rights Reserved.

estimated by the internal Rossby radius (~20–30 km in our domain), while wind stress curl-driven upwelling is prominent up to several hundred kilometers from shore and in the lee of coastal promontories. The nearshore band that emerges in EOF patterns must therefore contain both coastal and curl-driven upwelling and does not imply that the two mechanisms are out of phase. The details of the cross-shore structure are also likely to be influenced by the resolution of both the ocean model and the surface winds.

At locations in the northern half of the domain (39–45°N), the CUI is a good indicator of both the mean (Figure 2) and variability of upwelling transport (r = 0.63–0.70). At 33 and 36°N, the CUI is too strong and is not significantly correlated with net upwelling ($r \sim 0.3$) but is significantly correlated with PC1 ($r \sim 0.5$), indicating that it represents nearshore upwelling better than total upwelling. At all latitudes, Ekman transport calculated from model winds is strongly correlated with model upwelling transport. We therefore conclude that while onshore geostrophic flow has a significant impact on mean upwelling transport south of 40°N, its effect on the interannual variability is less pronounced.

All of the North Pacific basin-scale indices examined here (ENSO, PDO, and NPGO) are significantly correlated with elements of upwelling variability along the US West Coast. In contrast with prior studies indicating such correlations, we have shown that climate variability is associated not just with net upwelling changes but also with specific spatial distributions of vertical transport. In particular, positive (negative) phases of the NPGO (PDO) favor more intense upwelling within 50 km of shore, while negative (positive) phases are associated with a larger upwelling contribution farther offshore. As weak, widespread upwelling and intense localized upwelling each promote distinct biological communities [*Rykaczewski and Checkley*, 2008], the ecological implications of such correlations are an important topic for further study. For example, positive NPGO phases, associated with strong nearshore upwelling and presumably large nutrient flux from depth, may support a greater abundance of large plankton types, while weak upwelling associated with negative NPGO phases may support more small plankton. However, upwelling is just one driver of a complex biological response, and upwelling intensity, the focus of the present study, does not entirely govern the upwelled nutrient supply. Also important are the upwelling source depth and subsurface nutrient concentration. Source depth is modified by changes in stratification and surface wind structure [*Jacox and Edwards*, 2011, 2012] and is related to the PDO and NPGO [*Chhak and Di Lorenzo*, 2007; *Di Lorenzo et al.*, 2008], while nutrient depth profiles may be affected by local (e.g., wind) as well as remote (e.g., ENSO) forcing.

Finally, the question of whether trends observed here are indicative of multidecadal fluctuations or of long-term trajectories is clouded both by the length of the time series and by an increasing (decreasing) trend in the NPGO (PDO) during our study period. Extension of the current analysis to longer time scales, with appropriate atmospheric forcing and observational data, will help to clarify these issues and to distinguish the individual influences of the PDO and NPGO during periods when they are not so strongly correlated.

Acknowledgments
The model output used for analysis herein is available from oceanmodeling.ucsc.edu. This research was funded by NSF grant 1061434. We thank Clemente Tanajura and Will Crawford for many helpful discussions and two anonymous reviewers for comments that improved the clarity of the paper.

The Editor thanks two anonymous reviewers for their assistance in evaluating this paper.

References

Atlas, R., R. N. Hoffman, J. Ardizzone, S. M. Leidner, J. C. Jusem, D. K. Smith, and D. Gombos (2011), A cross-calibrated, multiplatform ocean surface wind velocity product for meteorological and oceanographic applications, *Bull. Am. Meteorol. Soc.*, *92*, 157–174, doi:10.1175/2010BAMS2946.1.

Auad, G., A. Miller, and E. Di Lorenzo (2006), Long-term forecast of oceanic conditions off California and their biological implications, *J. Geophys. Res.*, *111*, C09008, doi:10.1029/2005JC003219.

Bakun, A. (1973), Coastal upwelling indices, west coast of North America, 1946–71, *NOAA Tech. Rep., NMFS SSRF-671*, 103 pp., U.S. Dep. of Commer.

Bakun, A. (1990), Global climate change and intensification of coastal ocean upwelling, *Science*, *247*, 198–201.

Bograd, S. J., and R. J. Lynn (2001), Physical-biological coupling in the California Current during the 1997–99 El Niño–La Niña cycle, *Geophys. Res. Lett.*, *28*, 275–278, doi:10.1029/2000GL012047.

Broquet, G., C. A. Edwards, A. M. Moore, B. S. Powell, M. Veneziani, and J. D. Doyle (2009), Application of 4D-variational data assimilation to the California Current System, *Dyn. Atmos. Oceans*, *48*, 69–92.

Chavez, F. P., J. T. Pennington, C. G. Castro, J. P. Ryan, R. P. Michisaki, B. Schlining, P. Walz, K. R. Buck, A. McFadyen, and C. A. Collins (2002), Biological and chemical consequences of the 1997–1998 El Niño in central California waters, *Prog. Oceanogr.*, *54*, 205–232.

Chavez, F. P., J. P. Ryan, S. E. Lluch-Cota, and C. M. Ñiquen (2003), From anchovies to sardines and back: Multidecadal change in the Pacific Ocean, *Science*, *299*, 217–221, doi:10.1126/science.1075880.

Chenillat, F., P. Rivière, X. Capet, E. Di Lorenzo, and B. Blanke (2012), North Pacific Gyre Oscillation modulates seasonal timing and ecosystem functioning in the California Current upwelling system, *Geophys. Res. Lett.*, *39*, L01606, doi:10.1029/2011GL049966.

Chhak, K., and E. Di Lorenzo (2007), Decadal variations in the California Current upwelling cells, *Geophys. Res. Lett.*, *34*, L14604, doi:10.1029/2007GL030203.

Di Lorenzo, E., A. J. Miller, N. Schneider, and J. C. McWilliams (2005), The warming of the California Current: Dynamics and ecosystem implications, *J. Phys. Oceanogr.*, *35*, 336–362.

©2014. American Geophysical Union. All Rights Reserved.

Di Lorenzo, E., et al. (2008), North Pacific Gyre Oscillation links ocean climate and ecosystem change, *Geophys. Res. Lett.*, *35*, L08607, doi:10.1029/2007GL032838.

Dorman, C. E, and C. D. Winant (1995), Buoy observations of the atmosphere along the west coast of the United States, 1981–1990, *J. Geophys. Res.*, *100*(C8), 16,029–16,044.

García-Reyes, M., and J. Largier (2010), Observations of increased wind-driven coastal upwelling off central California, *J. Geophys. Res.*, *115*, C04011, doi:10.1029/2009JC005576.

García-Reyes, M., and J. Largier (2012), Seasonality of coastal upwelling off central and northern California: New insights, including temporal and spatial variability, *J. Geophys. Res.*, *117*, C03028, doi:10.1029/2011JC007629.

Ingleby, B., and M. Huddleston (2007), Quality control of ocean temperature and salinity profiles—Historical and real-time data, *J. Mar. Syst.*, *65*, 158–175.

Jacox, M. G., and C. A. Edwards (2011), Effects of stratification and shelf slope on nutrient supply in coastal upwelling regions, *J. Geophys. Res.*, *116*, C03019, doi:10.1029/2010JC006547.

Jacox, M. G., and C. A. Edwards (2012), Upwelling source depth in the presence of nearshore wind stress curl, *J. Geophys. Res.*, *117*, C05008, doi:10.1029/2011JC007856.

Macías, D., M. R. Landry, A. Gershunov, A. J. Miller, and P. J. S. Franks (2012), Climatic control of upwelling variability along the western North-American coast [online], *PLoS One*, *7*, e30436, doi:10.1371/journal.pone.0030436.

Mantua, N. J., S. R. Hare, Y. Zhang, J. M. Wallace, and R. C. Francis (1997), A Pacific interdecadal climate oscillation with impacts on salmon production, *Bull. Am. Meteorol. Soc.*, *78*, 1069–1079.

Marchesiello, P., and P. Estrade (2010), Upwelling limitation by onshore geostrophic flow, *J. Mar. Res.*, *68*, 37–62, doi:10.1357/002224010793079004.

Moore, A. M., H. G. Arango, G. Broquet, B. S. Powell, A. T. Weaver, and J. Zavala-Garay (2011a), The Regional Ocean Modeling System (ROMS) 4-dimensional variational data assimilation systems: Part I—System overview and formulation, *Prog. Oceanogr.*, *91*, 34–49.

Moore, A. M., H. G. Arango, G. Broquet, C. Edwards, M. Veneziani, B. Powell, D. Foley, J. D. Doyle, D. Costa, and P. Robinson (2011b), The Regional Ocean Modeling System (ROMS) 4-dimensional variational data assimilation systems: Part II—Performance and application to the California Current System, *Prog. Oceanogr.*, *91*, 50–73.

Moore, A. M., C. Edwards, J. Fiechter, P. Drake, H. G. Arango, E. Neveu, S. Gürol, and A. T. Weaver (2013), A 4D-Var analysis system for the California Current: A prototype for an operational regional ocean data assimilation system, in *Data Assimilation for Atmospheric, Oceanic and Hydrologic Applications*, vol. 2, edited by S. K. Park and L. Xu, pp. 345–366, Springer, Berlin, Heidelberg.

Palacios, D. M., S. J. Bograd, R. Mendelssohn, and F. B. Schwing (2004), Long-term and seasonal trends in stratification in the California Current, 1950–1993, *J. Geophys. Res.*, *109*, C10016, doi:10.1029/2004JC002380.

Rykaczewski, R. R., and D. M. Checkley (2008), Influence of ocean winds on the pelagic ecosystem in upwelling regions, *Proc. Natl. Acad. Sci.*, *105*, 1965–1970.

Schwing, F. B., M. O'Farrell, J. M. Steger, and K. Baltz (1996), Coastal upwelling indices, West Coast of North America, 1946–95, *Rep. NOAA-TM-NMFS-SWFSC-231*, U.S. Dep. of Commer.

Schwing, F. B., and R. Mendelssohn (1997), Increased coastal upwelling in the California Current System, *J. Geophys. Res.*, *102*, 3421–3438.

Schwing, F. B., T. Murphree, L. deWitt, and P. M. Green (2002), The evolution of oceanic and atmospheric anomalies in the northeast Pacific during the El Niño and La Niña events of 1995–2001, *Prog. Oceanogr.*, *54*, 459–491.

Seo, H., K. H. Brink, C. E. Dorman, D. Koracin, and C. A. Edwards (2012), What determines the spatial pattern in summer upwelling trends on the U.S. West Coast?, *J. Geophys. Res.*, *117*, C08012, doi:10.1029/2012JC008016.

Veneziani, M., C. A. Edwards, J. D. Doyle, and D. Foley (2009), A central California coastal ocean modeling study: 1. Forward model and the influence of realistic versus climatological forcing, *J. Geophys. Res.*, *114*, C04015, doi:10.1029/2008JC004774.

Wolter, K., and M. S. Timlin (1993), Monitoring ENSO in COADS with a seasonally adjusted principal component index, paper presented at 17th Climate Diagnostics Workshop, pp. 52–57, NOAA/NMC/CAC, NSSL, Okla. Clim. Surv., CIMMS and the School of Meteorol., Univ. of Oklahoma, Norman, Okla.

©2014. American Geophysical Union. All Rights Reserved.